Transport properties of stage-1 magnetic random-mixture graphite intercalation compounds

1996 J. Phys.: Condens. Matter 8 199

(http://iopscience.iop.org/0953-8984/8/2/008)

J. Phys.: Condens. Matter **8** (1996) 199–216. Printed in the UK

Transport properties of stage-1 magnetic random-mixture graphite intercalation compounds

Masatsugu Suzuki, Itsuko S Suzuki, Brian Olson† and Takehiko Shima

Department of Physics, State University of New York at Binghamton, Binghamton, NY 13902-6016, USA

Received 15 August 1995

Abstract. We have measured the temperature dependence of the in-plane electrical resistivity for stage-1 $Co_cMn_{1-c}Cl_2$ GICs ($0.70 \leqslant c \leqslant 1$) and stage-1 $Co_cMg_{1-c}Cl_2$ GICs ($0.85 \leqslant c \leqslant 1$) in the temperature range between 2.6 and 300 K. The resistivity shows a drastic increase with decreasing temperature below the critical temperature T_c for stage-1 $Co_cMn_{1-c}Cl_2$ GICs ($c \geqslant 0.85$) and stage-1 $Co_cMg_{1-c}Cl_2$ GICs ($c \geqslant 0.90$). The temperature dependence of this resistivity anomaly is described by a smeared power law with an exponent 2β, where β is the critical exponent of the spontaneous magnetization. This anomaly is explained in terms of a model based on the π–d exchange interaction between π-electrons in the graphite layers and spins in the intercalate layers. Below T_c, two-dimensional (2D) ferromagnetic intercalate layers are antiferromagnetically stacked along the c-axis. The π-electrons are scattered by spin fluctuations of a virtual antiferromagnetic in-plane spin configuration arising from the superposition of two ferromagnetic in-plane structures with spin directions antiparallel to each other. The Co concentration dependence of T_c for stage-1 $Co_cMg_{1-c}Cl_2$ GICs is also discussed in the light of the 2D percolation problem.

1. Introduction

Recently the transport properties of magnetic graphite intercalation compounds (GICs) such as $CoCl_2$ GIC and $NiCl_2$ GIC near the magnetic phase transition point T_c have excited considerable interest because of their two-dimensional (2D) electrical conduction [1]. Several research groups [2–6] have reported a drastic increase of the in-plane resistivity ρ_a for the stage-1 $CoCl_2$ GIC with decreasing temperature below T_c. Similar anomalous resistivity behaviours have been observed in the stage-1 $NiCl_2$ GIC [7, 8] and stage-1 $Co_cMg_{1-c}Cl_2$ GICs [9]. In contrast, the magnitude of the anomaly in ρ_a for the stage-2 $CoCl_2$ GIC near T_c is much smaller than that for the stage-1 $CoCl_2$ GIC. Sugihara *et al* [10] have proposed a theoretical model explaining the temperature dependence of ρ_a for stage-1 and stage-2 $CoCl_2$ GICs near T_c. They have shown that the drastic increase of ρ_a near T_c for the stage-1 $CoCl_2$ GIC is due to the scattering of π-electrons by Co^{2+} spins in the $CoCl_2$ layers through the π–d exchange interaction defined by

$$\mathcal{H}_{\pi-d} = -\sum_{\boldsymbol{R}} J_{\pi-d}(\boldsymbol{r}-\boldsymbol{R})\boldsymbol{s}_{\boldsymbol{r}} \cdot \boldsymbol{S}_{\boldsymbol{R}} \tag{1}$$

where $\boldsymbol{S}_{\boldsymbol{R}}$ and $\boldsymbol{s}_{\boldsymbol{r}}$ are the spins of Co^{2+} at the position $\boldsymbol{R}$ and the π-electron at $\boldsymbol{r}$, respectively. The semiempirical constant $J_{\pi-d}$ $(= |\epsilon|^2 J_{\pi-Cl})$ can be described in terms

† Present address: Department of Physics, Case Western Reserve University, Cleveland, OH 44106, USA.

0953-8984/96/020199+18$19.50

of indirect interactions through the admixture of Co^{2+}–Cl^{-} wave functions and Cl^{-}–C wave functions, where $\epsilon = b/U$, b is the transfer integral for transfer between Co and Cl, U is the energy difference between the excited and the ground state for the Co–Cl units without the presence of π-electrons, and $J_{\pi-Cl}$ is the exchange interaction between the π-electron and an unpaired 3p electron of Cl. Sugihara *et al* [10] have shown that the π–d exchange interaction results in two effects on the scattering of π-electrons. One effect is spin-disorder scattering. The other is a Fermi surface modification effect which becomes dominant for the stage-1 $CoCl_2$ GIC. The additional magnetic periodicity along the c-axis gives rise to a zone-folding effect. The Fermi surface is split into two Fermi surfaces as a result of the energy gap formation in the k_z-axis energy dispersion relation. This Fermi surface modification enhances the scattering probability of π-electrons because of a reduction in the screening of the charged scattering centres.

In the present work we have studied the transport properties of some magnetic random-mixture graphite intercalation compounds (RMGICs): stage-1 $Co_cM_{1-c}Cl_2$ GICs (M = Mn and Mg). The Co^{2+} and M^{2+} ions are randomly distributed on the triangular lattice in the same intercalate layers. The magnetic phase transitions of stage-2 RMGICs have been extensively studied by dc and ac magnetic susceptibility, and SQUID magnetization [11–13]. The magnetic phase transition of stage-1 RMGICs is similar to that of stage-2 RMGICs. In stage-2 $Co_cMn_{1-c}Cl_2$ GICs [12, 13] the spin frustration effect arises from a competition between ferromagnetic and antiferromagnetic intraplanar exchange interactions. In stage-1 [9] and stage-2 $Co_cMg_{1-c}Cl_2$ GICs [11] the dilution of Co^{2+} spins with nonmagnetic Mg^{2+} ions gives rise to a 2D percolation problem.

In section 3 we propose a model which can explain the temperature dependence of in-plane resistivity for stage-1 and stage-2 $CoCl_2$ GICs near T_c. Our model is rather different from the model of Sugihara *et al* [10] although both models take account of the π–d exchange interactions. Our model is based on the following idea. While the spin fluctuation of an ideal 2D ferromagnet does not contribute to the resistivity because there is no significant contribution of the forward scattering to the resistivity, the spin fluctuation of the 2D antiferromagnet gives rise to a drastic change of the resistivity near T_c because of the enhanced staggered mode. The π-electrons in the graphite layers are weakly coupled with Co^{2+} spins in the intercalate layers through the π–d exchange interaction. The π-electrons are scattered by the spin fluctuations of the ferromagnetic in-plane spin configuration for a stage-2 $CoCl_2$ GIC, and by the spin fluctuations of the antiferromagnetic spin configuration for a stage-1 $CoCl_2$ GIC, which is formed by the superposition of two in-plane ferromagnetic spin configurations with spins aligned antiparallel to each other. In stage-1 $Co_cM_{1-c}Cl_2$ GICs the superimposed in-plane spin configurations are expected to be much more complicated because of the additional effects such as (i) the degree of random distribution of spins in the intercalate layers and (ii) the combination of intraplanar exchange interactions, J(Co–Co) between Co^{2+} spins and J(Mn–Mn) between Mn^{2+} spins for stage-1 $Co_cMn_{1-c}Cl_2$ GICs.

In section 4 we present the experimental results on the temperature dependence of the in-plane resistivity ρ_a for stage-1 $Co_cM_{1-c}Cl_2$ GICs in the temperature range between 2.6 and 300 K. In section 5 the temperature dependence of ρ_a for stage-1 $Co_cM_{1-c}Cl_2$ GICs near T_c are examined and discussed in light of our model. The temperature dependence of ρ_a for stage-1 $Co_cM_{1-c}Cl_2$ GICs at high temperatures is also discussed in comparison with a conventional theory in which ρ_a is described by the equation $\rho_a = A_n + B_nT + C_nT^2$, where A_n, B_n, and C_n are constants.

2. Experimental procedure

Single crystals of $Co_cM_{1-c}Cl_2$ as intercalants were prepared by heating a mixture containing c of $CoCl_2$ to $(1-c)$ of MCl_2 in vacuum at $T = 780$ °C. The samples of $Co_cM_{1-c}Cl_2$ GICs were synthesized by heating single-crystal kish graphites (SCKG) and single-crystal $Co_cM_{1-c}Cl_2$ in a chlorine gas atmosphere with a pressure of 740 Torr. The reaction was continued at 450–560 °C for 20 days. The c-axis stacking sequence of $Co_cM_{1-c}Cl_2$ GIC samples used in the present work was confirmed to be a stage-1 sequence from $(00L)$ x-ray diffraction with a Huber double-circle diffractometer with a Mo Kα x-ray radiation source (1.5 kW) and a HOPG monochromator.

We determined the Co concentration of stage-1 $Co_cMn_{1-c}Cl_2$ GICs from electron microprobe measurement with the use of a scanning electron microscope (Model Hitachi S-450 and JOEL JXA-8900M). The electrons having a kinetic energy of 20 keV penetrate the sample to a depth of the order of 2 μm, spreading out a similar distance. The concentration (c_e) is the average concentration over several different points of the sample surface. We find that the actual Co concentration c_e of stage-1 $Co_cMn_{1-c}Cl_2$ GICs is in good agreement with the nominal Co concentration in the ranges of $0 < c \leqslant 0.4$ and $0.7 \leqslant c < 1$. The deviation of c_e from the nominal concentration for $0.4 < c < 0.7$ may be due to the limited energy resolution of electron microprobe analysis: a small peak of the Mn Kβ line at 6.492 keV and a large peak of the Co Kα line at 6.925 keV are superimposed [12].

We determined the Co concentration of stage-1 $Co_cMg_{1-c}Cl_2$ GICs by dc magnetic susceptibility investigation. The measurement was made by the Faraday balance method in the temperature range between 50 K and 300 K. A magnetic field of $H = 2$ kOe was applied in an arbitrary direction in the c-plane (the plane perpendicular to the c-axis). The actual Co concentration of stage-1 $Co_cMg_{1-c}Cl_2$ GICs is related to the Curie–Weiss temperature $\Theta(c)$ by the relation $c = \Theta(c)/\Theta(c=1)$ with $\Theta(c=1) = 23.20$ K. This relation is predicted from the molecular-field theory when Co^{2+} and Mg^{2+} ions are randomly distributed on the triangular lattice sites. We find that the nominal Co concentration is in good agreement with the actual concentration estimated from $\Theta(c)$ [11]. The stoichiometry ($C_nCo_cM_{1-c}Cl_2$) of each sample was determined from weight uptake measurements: typically $n = 5.76$ for the stage-1 $CoCl_2$ GIC, 5.37 for the stage-1 $Co_{0.80}Mn_{0.20}Cl_2$ GIC, and 6.52 for the the stage-1 $Co_{0.95}Mg_{0.05}Cl_2$ GIC. The ideal stoichiometry is approximated by $C_{4.1}Co_cM_{1-c}Cl_2$.

We measured the in-plane electrical resistivity of stage-1 $Co_cM_{1-c}Cl_2$ GICs using the conventional four-probe method. The samples each had a rectangular form with typically a base of 7 mm × 2 mm and a height of 0.5 mm. Four thin gold wires (25 μm diameter)—acting as the current and voltage probes—were attached to one base of the sample by silver paste (4922N, Du Pont), which was diluted with 2-butoxyethyl acetate; voltage probes were located between the current probes. The sample was mounted on a surface of copper heat sink which was electrically insulated with a varnish (GE-7031). The current (typically 1–50 mA) was supplied through the current probes by a programmable current source (Keithley, Model 224). The voltage generated across the voltage probes was measured by a digital nanovoltmeter (Keithley, Model 181). For each temperature T the voltage across the voltage probes was measured for the forward and reverse current directions, alternating between them three times. The averages of the data for forward and reverse current directions are denoted by V^+ (> 0) and V^- (< 0), respectively. The voltage data were calculated as $V = (V^+ - V^-)/2$. The temperatures of the samples were measured using a silicon diode sensor (DT-470-SD13, Lake Shore) embedded in the copper heat sink, which was supplied by a 10 μA current source. The ρ_a versus T data were taken through an IEEE 488 bus to a computer. Note that the absolute value of the resistivity cannot be

exactly determined by the four-probe method used here. The measured resistivity is very sensitive to the location of probes, the area of silver paste on the sample surface, the distance between voltage probes, and so on. Thus we report only the normalized in-plane resistivity data, defined by $\zeta(T)$ $(= \rho_a(T)/\rho_a(290\ \mathrm{K}))$, which is independent of the above factors.

3. The model

3.1. The conduction mechanism in stage-1 and stage-2 $CoCl_2$ GICs

The c-axis stacking sequence of $CoCl_2$ layers in a stage-1 $CoCl_2$ GIC is different from that in a stage-2 $CoCl_2$ GIC. For the stage-1 $CoCl_2$ GIC the $CoCl_2$ layers stack in an ordered abgabg rhombohedral sequence [14], while for the stage-2 $CoCl_2$ GIC the $CoCl_2$ layers are structurally uncorrelated along the c-axis [14, 15]. Here the translation of the α-$CoCl_2$ layer by the vectors $\boldsymbol{\delta}$ $(=(2\boldsymbol{a}+\boldsymbol{b})/3)$ and $-\boldsymbol{\delta}$ gives rise to β- and γ-$CoCl_2$ layers, respectively, where $\boldsymbol{a}$ and $\boldsymbol{b}$ are the primitive lattice vectors: $|\boldsymbol{a}| = |\boldsymbol{b}| = 3.572$ Å [14] and the angle between $\boldsymbol{a}$ and $\boldsymbol{b}$ is 120°.

For both stage-1 and stage-2 $CoCl_2$ GICs the Co^{2+} spins in each $CoCl_2$ layer become 2D ferromagnetically ordered at low temperatures. Below T_c, these 2D ferromagnetic layers are antiferromagnetically stacked along the c-axis [16, 17]. When the π-electrons in the graphite layers are magnetically coupled with Co^{2+} spins of the $CoCl_2$ layers through a π–d exchange interaction, the electrical conduction of π-electrons is expected to be influenced by long-range in-plane spin ordering of $CoCl_2$ layers. For the stage-2 $CoCl_2$ GIC the π-electrons experience a molecular field from Co^{2+} spins of the nearest-neighbour (N.N.) $CoCl_2$ layer. The molecular field from Co^{2+} spins of the next-nearest-neighbour (N.N.N.) $CoCl_2$ layer is much weaker than that of the N.N. $CoCl_2$ layer. Note that these two $CoCl_2$ layers are structurally uncorrelated with each other. Thus the π-electrons are scattered by ferromagnetically ordered Co^{2+} spins in the $CoCl_2$ layer (the 2D ferromagnet). In contrast, for the stage-1 $CoCl_2$ GIC the π-electrons experience two kinds of molecular field which are antiparallel to each other. These types of molecular field arise from the Co^{2+} spins of two adjacent $CoCl_2$ layers next to the graphite layer, where these two $CoCl_2$ layers are structurally correlated. For π-electrons the π–d interaction effect from Co^{2+} spins in one N.N. $CoCl_2$ layer is exactly the same as that in the other N.N. $CoCl_2$ layer. This implies that the scattering of π-electrons by Co^{2+} spins is equivalent to that of Co^{2+} spins in the resultant antiferromagnetic in-plane spin configuration which is formed by the superposition of the two N.N. in-plane ferromagnetic spin configurations.

In figures 1(a) and 1(b) we schematically show the π–d exchange interaction between a π-electron in the graphite layer and Co^{2+} spins in α- and β-$CoCl_2$ layers for the stage-1 $CoCl_2$ GIC. As shown in figure 1(b), the π-electrons in the graphite layer can be treated as if they are scattered by antiferromagnetically ordered Co^{2+} spins in one $CoCl_2$ layer (the 2D antiferromagnet), which is located at a distance 4.72 Å from the graphite layer.

3.2. Resistivity due to spin-fluctuation scattering

In the acceptor GICs it is well known that the c-axis resistivity is much larger than the in-plane resistivity because the adjacent graphite layers are separated by insulating intercalate layers [1]. This implies that the 2D electrical conduction occurs in the graphite layers. The electrical resistivity of our system can be analysed using the formula

$$\rho_a(T) = \rho_s(T) + \rho_n(T) \tag{2}$$

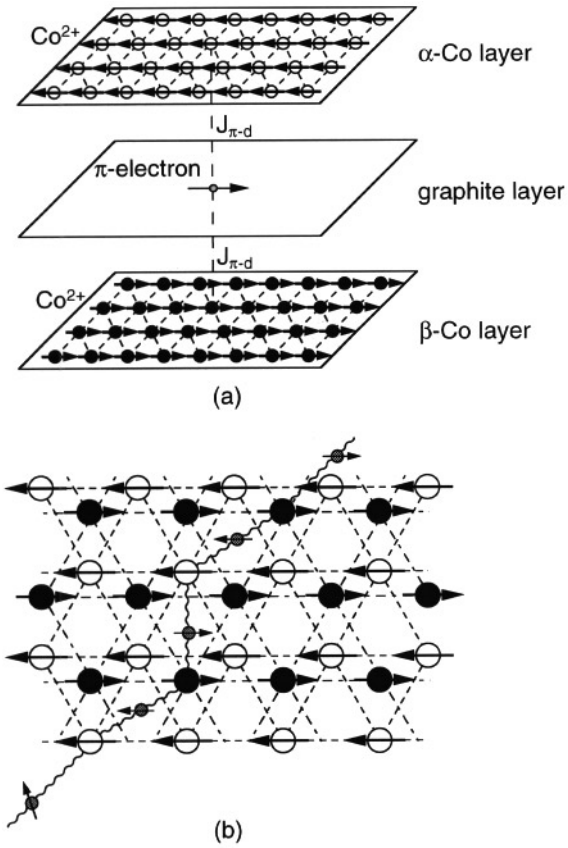

Figure 1. (a) A schematic diagram of π–d exchange interaction between π-electrons and Co^{2+} spins in α- and β-$CoCl_2$ layers for a stage-1 $CoCl_2$ GIC. (b) A schematic diagram for the scattering of π-electrons in the graphite layer by an in-plane antiferromagnetic spin structure located at a distance of 4.72 Å from the graphite layer.

where $\rho_s(T)$ is the magnetic resistivity due to spin-fluctuation scattering and $\rho_n(T)$ is the sum of residual resistivity due to the scattering by impurities and lattice defects and the resistivity due to the electron–phonon scattering. The resistivity $\rho_n(T)$ is described by

$$\rho_n(T) = A_n + B_n T + C_n T^2 \tag{3}$$

where A_n is the residual resistivity, and the $B_n T$- and $C_n T^2$-terms (B_n and C_n are constants) are the contributions due to the electron–phonon scattering. The Fermi surfaces of these compounds each consist of two kinds of cylindrical surface called pockets. The T- and T^2-terms originate from the intrapocket scattering of carriers by phonons with small wave numbers and the interpocket scattering by phonons with large wave numbers, respectively [18].

Here we consider the magnetic resistivity $\rho_s(T)$ in the case when the π-electrons in the graphite layer are scattered by a 2D ferromagnetic system or a 2D antiferromagnetic system (see figure 1(b)). The resistivity $\rho_s(T)$ is described as

$$\rho_s = \frac{m}{ne^2\tau_s} \tag{4}$$

where m is the effective mass of an electron and n is the electron concentration. The relaxation time τ_s associated with the scattering from 2D spin fluctuations [19–22] is defined by

$$\frac{1}{\tau_s} = \frac{\hbar k_F}{m} 2\int_0^{\pi} \frac{\mathrm{d}\sigma}{\mathrm{d}\theta}(1-\cos\theta)\ \mathrm{d}\theta \tag{5}$$

where k_F is the Fermi wave number of the 2D Fermi surface and θ ($=\theta_{k,k'}$) is the scattering angle between the in-plane wave vectors of incoming ($\boldsymbol{k}$) and outgoing electrons ($\boldsymbol{k}'$). We note that (4) and (5) are valid irrespective of the separation distance between the graphite layer and the intercalate layer, if there are π–d exchange interactions between π-electrons and Co^{2+} spins. For single-particle elastic scattering, the differential scattering cross section per magnetic spin in the Born approximation is given by

$$\frac{\mathrm{d}\sigma}{\mathrm{d}\theta} = \left(\frac{\sigma_0}{2\pi}\right)\sum_{\boldsymbol{R}} \frac{\Gamma(\boldsymbol{R})}{S(S+1)}\exp(\mathrm{i}\boldsymbol{Q}\cdot\boldsymbol{R}) = \left(\frac{\sigma_0}{2\pi}\right)\frac{\Gamma(\boldsymbol{Q})}{S(S+1)} \tag{6}$$

where σ_0 is defined by

$$\sigma_0 = \frac{1}{4\pi}\left(\frac{mJ_{\pi-d}}{\hbar^2}\right)^2 S(S+1) \tag{7}$$

and where $\boldsymbol{Q}$ ($=\boldsymbol{k}-\boldsymbol{k}'$) is the scattering wave vector, and $\Gamma(\boldsymbol{Q})$ is the Fourier transform of the static spin correlation function for two spins separated by a distance $\boldsymbol{R}$:

$$\Gamma(\boldsymbol{R}) = \langle \boldsymbol{S}_0 \cdot \boldsymbol{S}_R \rangle. \tag{8}$$

It is useful to define spin variables $\boldsymbol{S}_q$ in the reciprocal-lattice space as the Fourier transforms of the corresponding real-space spin variables $\boldsymbol{S}_R$:

$$\boldsymbol{S}_R = \frac{1}{\sqrt{N}}\sum_{\boldsymbol{q}} \exp(-\mathrm{i}\boldsymbol{q}\cdot\boldsymbol{R})\boldsymbol{S}_q \qquad \boldsymbol{S}_q = \frac{1}{\sqrt{N}}\sum_{\boldsymbol{R}} \exp(\mathrm{i}\boldsymbol{q}\cdot\boldsymbol{R})\boldsymbol{S}_R. \tag{9}$$

Then $\Gamma(\boldsymbol{Q})$ can be rewritten as

$$\Gamma(\boldsymbol{Q}) = \langle \boldsymbol{S}_{\boldsymbol{Q}} \cdot \boldsymbol{S}_{-\boldsymbol{Q}} \rangle. \tag{10}$$

In the high-temperature limit $\Gamma(\boldsymbol{Q})$ is equal to $S(S+1)$. The resistivity of the system due to the π–d exchange interaction is given by

$$\rho_s = \frac{1}{\pi}\rho_s^0 \int_0^{\pi} \mathrm{d}\theta\ (1-\cos\theta)\Gamma(\boldsymbol{Q}) \tag{11}$$

where ρ_s^0 is the resistivity in the high-temperature limit and is defined as

$$\rho_s^0 = \frac{\hbar k_F}{4\pi n}\left(\frac{mJ_{\pi-d}}{e\hbar^2}\right)^2 S(S+1). \tag{12}$$

Here we consider only elastic scattering. Since $|\boldsymbol{k}| = |\boldsymbol{k}'| = k_F$ and $\boldsymbol{Q} = \boldsymbol{k} - \boldsymbol{k}'$, we have the relation $Q = |\boldsymbol{Q}| = 2k_F \sin(\theta/2)$. The resistivity can be rewritten as

$$\rho_s = \frac{\rho_s^0}{\pi k_F^2}\int_0^{2k_F} \mathrm{d}Q\ f(Q)\Gamma(\boldsymbol{Q}) \tag{13}$$

where $f(Q)$ is defined by

$$f(Q) = \frac{Q^2}{\sqrt{4k_F^2 - Q^2}}. \tag{14}$$

The function $f(Q)$ is equal to zero at $Q = 0$ and then monotonically increases with increasing Q.

3.3. Resistivity of the 2D ferromagnet and the 2D antiferromagnet

On the basis on the above formulation we predict the temperature dependence of electrical resistivity for ideal 2D ferromagnetic and 2D antiferromagnetic systems. For the ferromagnetic system, the spin correlation function $\Gamma(\boldsymbol{Q})$ above T_c coincides with the wave-vector-dependent susceptibility $\chi(\boldsymbol{Q})$ [23–25], and it can be described as

$$\Gamma(\boldsymbol{Q}) = \chi(\boldsymbol{Q}) = \frac{\chi(\boldsymbol{Q}=0)}{1+|\boldsymbol{Q}|^2/\kappa^2} \tag{15}$$

near $\boldsymbol{Q}=0$, where κ is the inverse correlation length, $\chi(\boldsymbol{Q})$ is related to the static spin correlation between Co^{2+} spins in the same $CoCl_2$ layer, $\chi(\boldsymbol{Q}=0)=\chi_0 T$, and the susceptibility χ_0 is proportional to $\kappa^{-2+\eta}$. The parameter η ($\simeq 0$) is a Fisher–Burford critical exponent. Then the resistivity ρ_s is predicted to be $\rho_s = \kappa^3 \chi(\boldsymbol{Q}=0) \simeq \kappa^{1+\eta}$ which goes to zero on approaching T_c from above. The forward scattering with $\boldsymbol{Q}=0$ ($\boldsymbol{k}=\boldsymbol{k}'$) does not contribute to ρ_s because the factor $1-\cos\theta_{\boldsymbol{k},\boldsymbol{k}'}$ is zero. Below T_c, $\Gamma(\boldsymbol{Q})$ becomes

$$\Gamma(\boldsymbol{Q}) = \langle S_{Q=0}\rangle^2 \delta(\boldsymbol{Q}) + \chi(\boldsymbol{Q}) \tag{16}$$

where $\delta(\boldsymbol{Q})$ is a delta function with a sharp peak at $\boldsymbol{Q}=0$ and $\langle S_{Q=0}\rangle$ is proportional to the spontaneous magnetization M of the system. The magnetization M varies with temperature as described by $M \sim |t|^\beta$ below T_c, where $t=(T-T_c)/T_c$. Because of the properties of $\delta(\boldsymbol{Q})$ the first term of $\Gamma(\boldsymbol{Q})$ does not contribute to the resistivity ρ_s. Thus the resistivity is given by the form $\rho_s \simeq |t|^{\nu(1+\eta)}$ for $T > T_c$ and $\rho_s \simeq |t|^{\nu'(1+\eta')}$ for $T < T_c$, showing no anomaly around T_c. Here $\kappa \simeq |t|^\nu$ for $T > T_c$, and ν' and η' are the corresponding critical exponents for $T < T_c$. The situation is different for the 2D antiferromagnet. As the temperature approaches T_c from above the importance of the staggered mode ($\boldsymbol{Q}_0$) is enhanced [23], where $\boldsymbol{Q}_0$ is a wave vector for the in-plane antiferromagnetic Bragg point. The spin correlation function $\Gamma(\boldsymbol{Q})$ near $\boldsymbol{Q}=\boldsymbol{Q}_0$ can be written as [24, 25]

$$\Gamma(\boldsymbol{Q}) = \chi(\boldsymbol{Q}) = \frac{\chi(\boldsymbol{Q}_0)}{1+|\boldsymbol{Q}-\boldsymbol{Q}_0|^2/\kappa^2} \tag{17}$$

where $\chi(\boldsymbol{Q}=\boldsymbol{Q}_0)=\chi_s T$ and the staggered susceptibility χ_s diverges at T_c: $\chi_s \sim \kappa^{-2+\eta}$. Thus the resistivity ρ_s is predicted to be $\rho_s \simeq \kappa\chi(\boldsymbol{Q}=\boldsymbol{Q}_0) \simeq \kappa^{-1-\eta}$, or to take the form

$$\rho_s = \rho_2 |t|^{\nu(-1+\eta)} \qquad (T > T_c) \tag{18}$$

where ρ_2 is a constant with the dimension of resistivity. This form indicates that ρ_s diverges at T_c on approaching T_c from above since η is a small positive value. On the other hand, the spin correlation function $\Gamma(\boldsymbol{Q})$ below T_c can be described as [24, 25]

$$\Gamma(\boldsymbol{Q}) = \langle S_{\boldsymbol{Q}=\boldsymbol{Q}_0}\rangle^2 \delta(\boldsymbol{Q}-\boldsymbol{Q}_0) + \frac{\chi(\boldsymbol{Q}_0)}{1+|\boldsymbol{Q}-\boldsymbol{Q}_0|^2/\kappa^2} \tag{19}$$

where $\langle S_{\boldsymbol{Q}=\boldsymbol{Q}_0}\rangle$ is proportional to the staggered magnetization M_s of the system. The magnetization M_s varies with temperature as $|t|^\beta$ for $T < T_c$. Then the resistivity is given by a sum of the contributions related to the staggered magnetization and staggered susceptibility, or the form

$$\rho_s = \rho_1' |t|^{2\beta} + \rho_2' |t|^{\nu'(-1+\eta')} \qquad (T < T_c) \tag{20}$$

where ρ_1' and ρ_2' are constants with the dimension of resistivity. From (18) and (20) we conclude as follows. (i) In the case where $\rho_1' \gg \rho_2'$ the resistivity ρ_s drastically increases with decreasing temperature below T_c. (ii) In the case where $\rho_1' \ll \rho_2'$ the resistivity ρ_s shows a sharp peak at T_c. (iii) In the case where $\rho_1' \simeq \rho_2'$ the drastic increase of ρ_s below T_c is superimposed on a sharp peak at T_c. Here it should be noted that case (i) ($\rho_1' \gg \rho_2'$)

may describe the situation for the stage-1 $CoCl_2$ GIC because of very weak spin correlation between Co^{2+} spins in adjacent $CoCl_2$ layers. In this model we neglect the effect [21] whereby the spins separated by a distance greater than the electron mean free path cannot scatter π-electrons coherently. If this effect is appropriately included, the divergence of resistivity in (18) and (20) near T_c may be greatly reduced.

Here we discuss the effect of a magnetic field on the resistivity of a 2D antiferromagnet. When a magnetic field which is larger than a spin-flop field ($H_F \simeq 10$ Oe for the stage-2 $CoCl_2$ GIC [26]) is applied to any direction in the c-plane of this system, the importance of this staggered mode ($\boldsymbol{Q} = \boldsymbol{Q}_0$) is diminished while the importance of the $\boldsymbol{Q} = 0$ mode is enhanced, leading to the drastic decrease of resistivity as the magnetic field increases.

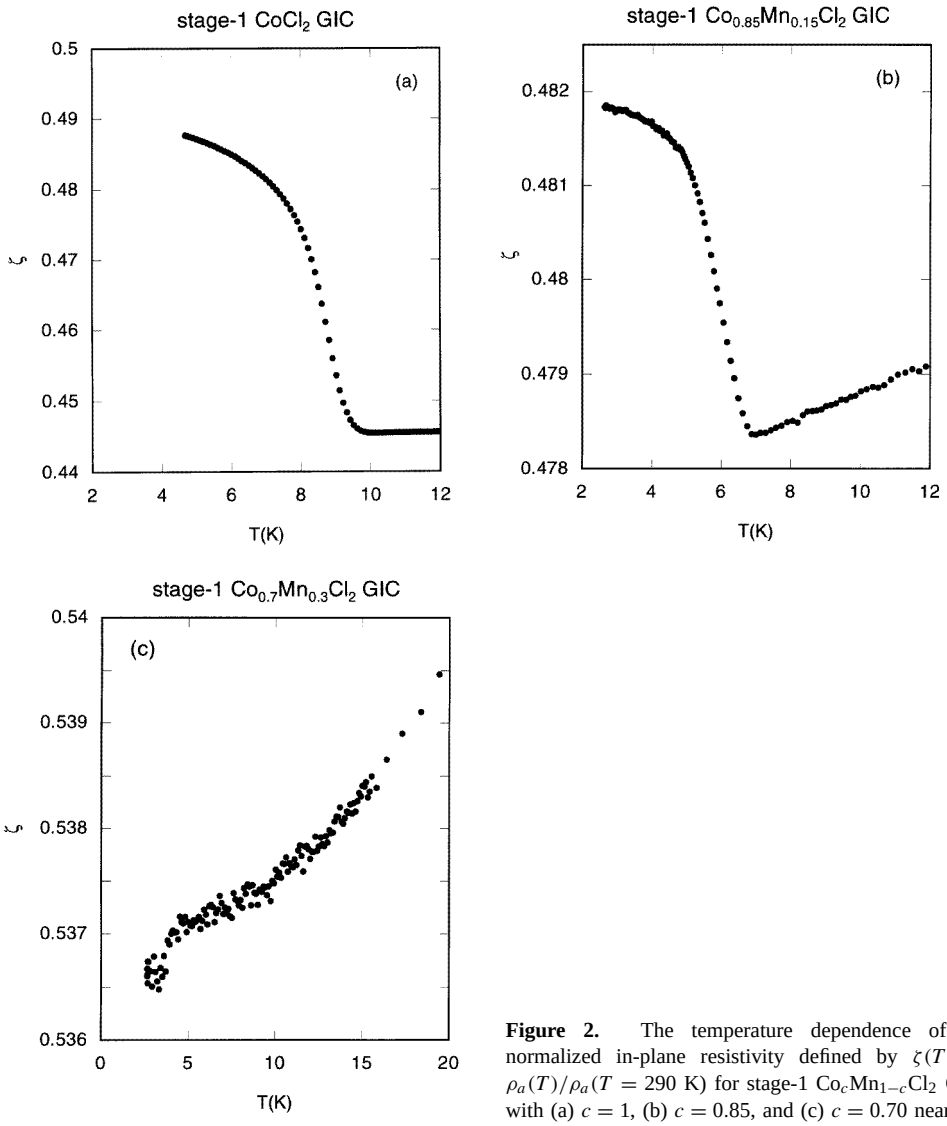

Figure 2. The temperature dependence of the normalized in-plane resistivity defined by $\zeta(T) = \rho_a(T)/\rho_a(T = 290\ \mathrm{K})$ for stage-1 $Co_cMn_{1-c}Cl_2$ GICs with (a) $c = 1$, (b) $c = 0.85$, and (c) $c = 0.70$ near T_c.

4. Results

4.1. Electrical resistivity of stage-1 $Co_cMn_{1-c}Cl_2$ GICs

We have measured the temperature dependence of the in-plane resistivity $\rho_a(T)$ of stage-1 $Co_cMn_{1-c}Cl_2$ GICs based on SCKG with $c = 1$, 0.90, 0.85, 0.80, and 0.70. Figure 2 shows typical examples of normalized in-plane resistivity defined by $\zeta(T)$ $(=\rho_a(T)/\rho_a(290\ \mathrm{K}))$ versus T for stage-1 $Co_cMn_{1-c}Cl_2$ GICs: (a) $c = 1$, (b) $c = 0.85$, and (c) $c = 0.70$ at low temperatures. For $c = 1$ the in-plane resistivity exhibits a drastic increase below $\simeq$10 K with decreasing temperature and almost reaches a saturated value at around 5 K. The relative value defined by

$$\Delta\tilde{\rho} = \left(\frac{\zeta_{sat}}{\zeta_{min}} - 1\right) \times 100\% \tag{21}$$

gives a measure of the degree of drastic increase in the in-plane resistivity, where ζ_{sat} and ζ_{min} are the saturated value of ζ at the lowest temperature and the minimum value of ζ, respectively. The value of $\Delta\tilde{\rho}$ is estimated to be 9.7% for $c = 1$ and is in good agreement with that reported by Yeh *et al* [2] (10%). For $c = 0.90$ the in-plane resistivity shows a drastic increase below $\simeq$8 K and reaches a saturated value at around 6 K: $\Delta\tilde{\rho}$ (=0.05%). For $c = 0.85$ (figure 2(b)) the in-plane resistivity also shows a drastic increase below $\simeq$6.9 K and reaches a saturated value near 2.6 K: $\Delta\tilde{\rho}$ (=0.7 %), which is much smaller than that for $c = 1$. For $c = 0.70$ the in-plane resistivity increases monotonically with increasing temperature, showing no anomaly at low temperatures. These results suggest that the value of $\Delta\tilde{\rho}$ rapidly decreases with decreasing Co concentration.

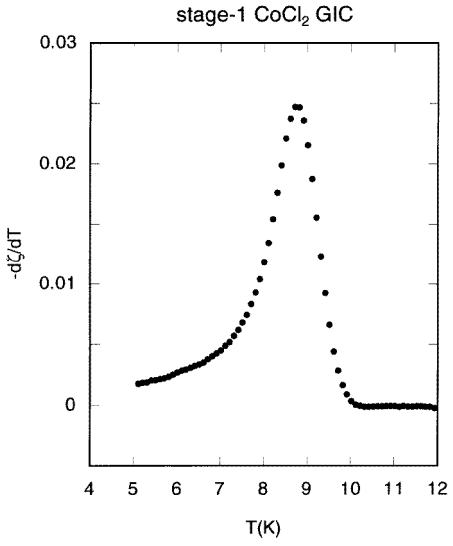

Figure 3. $-\mathrm{d}\zeta/\mathrm{d}T$ versus T for the stage-1 $CoCl_2$ GIC near T_c.

Figure 3 shows the temperature dependence of $-\mathrm{d}\zeta/\mathrm{d}T$ for $c = 1$. A sharp peak is observed at around 8.85 K. This peak temperature is close to the value of T_c determined from the ac magnetic susceptibility of the stage-2 $CoCl_2$ GIC: the ac susceptibility shows a sharp peak at T_c. Here we note that for $c = 1$ the temperature ($\simeq$10 K) at which ζ starts to rise is higher than T_c.

Figure 4 shows the temperature dependence of ζ for stage-1 $Co_cMn_{1-c}Cl_2$ GICs with (a) $c = 1$, (b) $c = 0.85$, and (c) $c = 0.70$ in the temperature range between 2.6 and

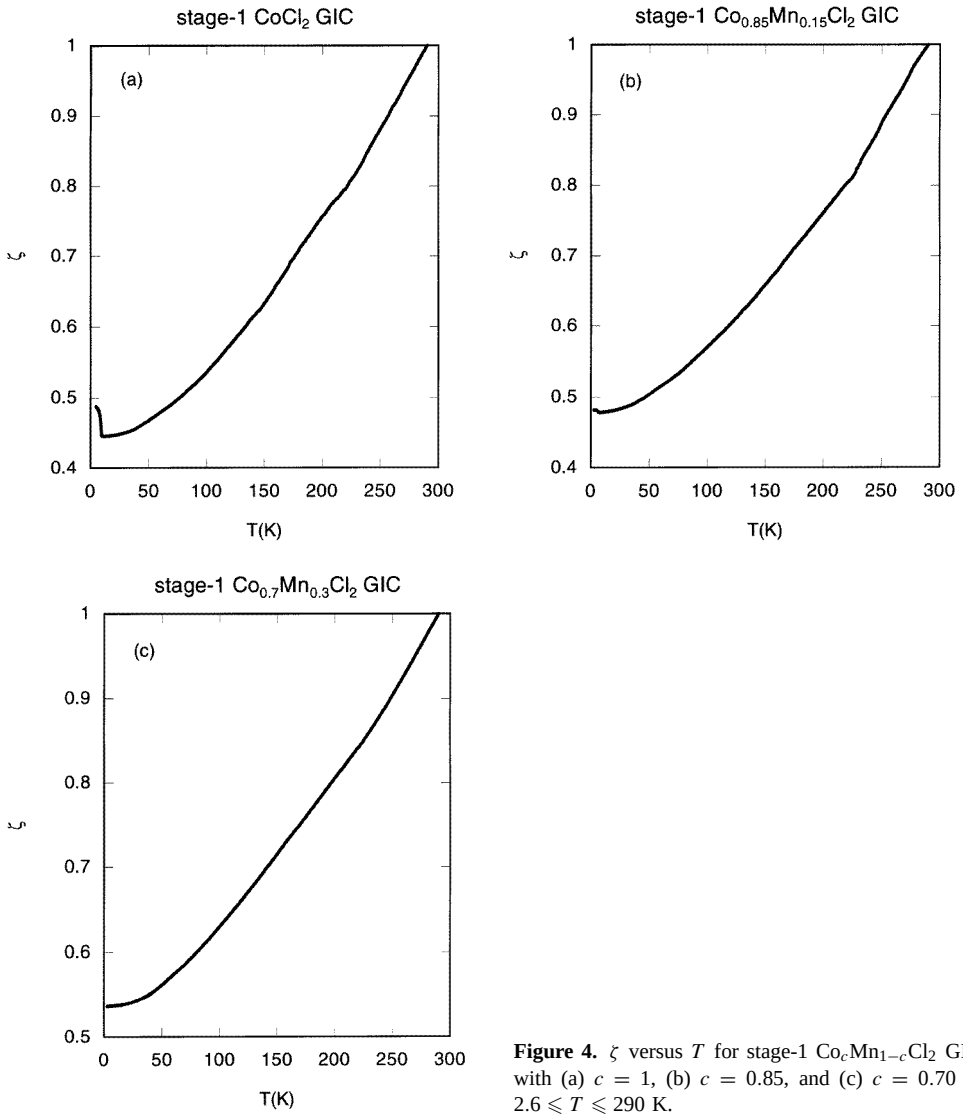

Figure 4. ζ versus T for stage-1 $Co_cMn_{1-c}Cl_2$ GICs with (a) $c = 1$, (b) $c = 0.85$, and (c) $c = 0.70$ for $2.6 \leqslant T \leqslant 290$ K.

290 K. We find that the magnitude of the drastic increase of ζ observed below 10 K clearly decreases with decreasing Co concentration, and that ζ increases monotonically with increasing temperature at least for $20 \leqslant T \leqslant 290$ K. The ζ–T data for stage-1 $Co_cMn_{1-c}Cl_2$ GICs fit very well to the form

$$\zeta(T) = A + BT + CT^2 \tag{22}$$

where the coefficients A, B, and C are listed in table 1. For comparison, the result for $c = 0.90$ is also shown in table 1. The characteristic temperature T_0 listed in table 1 is a temperature at which $BT = CT^2$. The T^2-term which is dominant for $T \gg T_0$ is due to the interpocket electron–phonon scattering, while the T-term which is dominant for $T \ll T_0$ is due to the intrapocket electron–phonon scattering. The interpocket transition is induced by the coupling of electrons to the phonon associated with the in-plane lattice vibration ($D \simeq 16$ eV) which is much larger than that associated with the out-of-plane vibration

($D < 3.7$ eV) [27]. Electron–electron scattering is ineffective as regards contributing to the resistivity. This temperature dependence of ρ_a is similar to that of nonmagnetic acceptor-type GICs such as $CdCl_2$ GIC with $T_0 = 96.6$ K [28]. Note that the values of T_0 are different for different samples as shown in table 1.

Table 1. The coefficients A, B, and C of the normalized in-plane resistivity ζ for stage-1 $Co_cM_{1-c}Cl_2$ GICs determined from a least-squares fit of the data (for $20 \leqslant T \leqslant 290$ K) to the form $\zeta(T) = \rho_a(T)/\rho_a(290\text{ K}) = A + BT + CT^2$. T_0 is the temperature at which $BT = CT^2$.

The stage-1 $Co_cMn_{1-c}Cl_2$ GIC				
c	A	B	C	T_0 (K)
1	0.428	6.599×10^{-4}	4.639×10^{-6}	142
0.90	0.685	8.292×10^{-4}	9.297×10^{-7}	892
0.85	0.460	6.972×10^{-4}	4.037×10^{-6}	172
0.70	0.507	1.010×10^{-3}	2.345×10^{-6}	431
The stage-1 $Co_cMg_{1-c}Cl_2$ GIC				
c	A	B	C	T_0 (K)
0.95	0.508	1.009×10^{-3}	2.480×10^{-6}	407
0.90	0.465	1.703×10^{-3}	4.045×10^{-7}	421

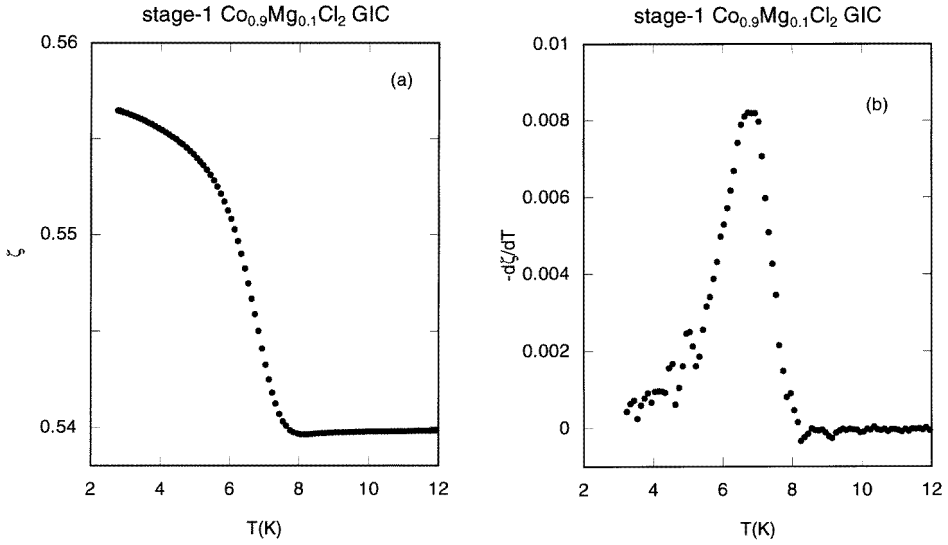

Figure 5. (a) ζ versus T and (b) $-\mathrm{d}\zeta/\mathrm{d}T$ versus T for the stage-1 $Co_cMg_{1-c}Cl_2$ GIC with $c = 0.90$ near T_c.

4.2. Electrical resistivity of stage-1 $Co_cMg_{1-c}Cl_2$ GICs

We have measured the temperature dependence of the in-plane resistivity ρ_a of stage-1 $Co_cMg_{1-c}Cl_2$ GICs on the basis of SCKG with $c = 0.95$, 0.90, and 0.85. Figure 5(a) shows the temperature dependence of ζ for the stage-1 $Co_cMg_{1-c}Cl_2$ GIC with $c = 0.9$, which is similar to that for $c = 1$ as shown in figure 2(a): it exhibits a drastic increase

at $\simeq$7.5 K with decreasing temperature. The magnitude of the increase $\Delta\tilde{\rho}$ (=3.1%) is much smaller than that for $c = 1$ (9.7%). Figure 5(b) shows the temperature dependence of $-\mathrm{d}\zeta/\mathrm{d}T$ for $c = 0.90$. A sharp peak is observed at around 6.85 K which is much lower than the value of T_c for the stage-1 $CoCl_2$ GIC (=8.85 K). This decrease of the peak temperature indicates that the long-range spin order is partly broken by the replacement of Co^{2+} ions by nonmagnetic Mg^{2+} ions.

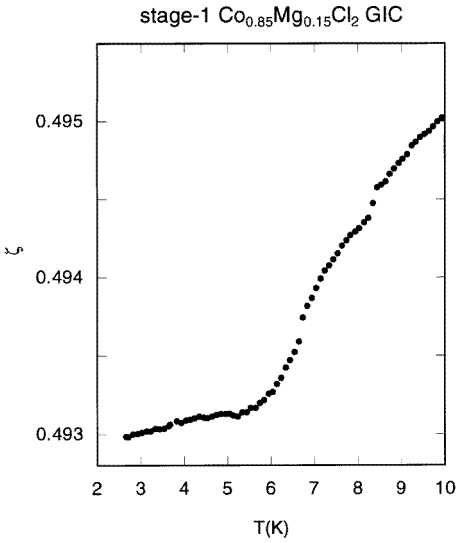

Figure 6. ζ versus T for the stage-1 $Co_cMg_{1-c}Cl_2$ GIC with $c = 0.85$ near T_c.

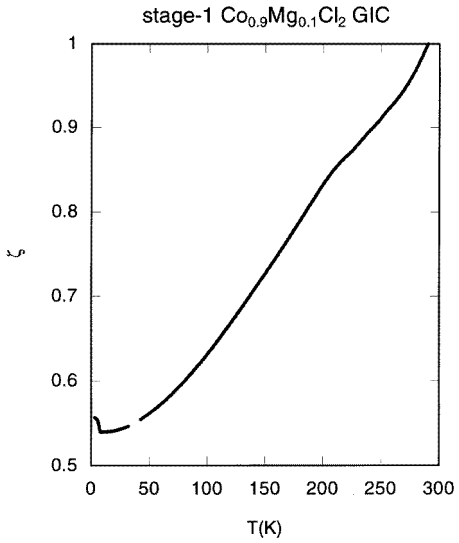

Figure 7. ζ versus T for stage-1 $Co_cMg_{1-c}Cl_2$ GICs with $c = 0.90$ for $2.6 \leqslant T \leqslant 290$ K.

Figure 6 shows the temperature dependence of ζ for $c = 0.85$. It is very different from that for 0.90: it gradually increases with increasing temperature for $2.6 \leqslant T \leqslant 5.8$ K and rapidly increases above 5.8 K with further increasing temperature. The kink temperature 5.8 K is considered to be close to T_c. In section 5 the Co concentration dependence of T_c will be further examined in a discussion of the percolation threshold of these systems. Note that the temperature dependence of ζ for $c = 0.85$ is different from that for $c = 0.77$ reported by Nicholls and Dresselhaus [9]: the resistivity begins to increase at $\simeq$4 K with decreasing temperature ($\Delta\tilde{\rho} = 1.5\%$).

Here we describe the temperature dependence of ζ for $c = 0.95$ which is not shown in figures 5(a) and 6. The temperature dependence of ζ for $c = 0.95$ is roughly similar to that for $c = 0.90$ as shown in figure 5(a): it exhibits a drastic increase at $\simeq$9 K ($\Delta\tilde{\rho} = 1.5\%$) with decreasing temperature. The temperature derivative of ζ shows a peak at around T_c (=8.59 K), which is lower than the temperature at which ζ starts to rise. Figure 7 shows the temperature dependence of ζ for stage-1 $Co_cMg_{1-c}Cl_2$ GICs with $c = 0.90$ for the temperature range between 2.6 and 290 K. The monotonic increase of ζ is observed for $20 \leqslant T \leqslant 290$ K as the temperature increases. A small shoulder-type anomaly observed near 210 K is considered to be related to some structural phase transition. A similar monotonic increase in ζ is also observed for $c = 0.95$; no resistivity anomaly is observed near 210 K. The least-squares fit of the ζ–T data for $c = 0.95$ and 0.90 to (22) yields the coefficients A, B, C, and T_0 listed in table 1.

5. Discussion

5.1. The temperature dependence of the in-plane resistivity

In section 3 we predicted the temperature dependence of the in-plane resistivity ρ_a for the stage-1 $CoCl_2$ GIC, which is described by (18) for $T > T_c$ and by (20) for $T < T_c$. The first term of (20) is related to the magnetic neutron scattering intensity of the antiferromagnetic Bragg peak at the wave vector $\boldsymbol{Q} = L\boldsymbol{c}^*$ with $L = 1/2$, where $\boldsymbol{c}^*$ ($|\boldsymbol{c}^*| = 2\pi/d$) is the fundamental reciprocal-lattice vector along the $(00L)$ direction and d is the c-axis repeat distance of the stage-1 $CoCl_2$ GIC. Equation (18) and the second term of (20) are related to the magnetic diffuse scattering intensity at around $\boldsymbol{Q} = \boldsymbol{c}^*/2$. Ikeda *et al* [29] have reported the experimental results on the magnetic neutron scattering of the stage-1 $CoCl_2$ GIC. The intensity at $\boldsymbol{Q} = \boldsymbol{c}^*/2$ drastically decreases with increasing temperature. It does not reduce to zero but shows a tail at around 9.9 K due to the smearing in T_c.

First we analyse the temperature dependence of the intensity at $\boldsymbol{Q} = \boldsymbol{c}^*/2$ by assuming that the smearing of T_c is described by a Gaussian distribution function with the average value $\langle T_c \rangle$ and width σ [30]:

$$f(T_c) = \frac{1}{\sqrt{2\pi}\sigma} \exp\left[-\frac{1}{2}\left(\frac{T_c - \langle T_c \rangle}{\sigma}\right)^2\right]. \tag{23}$$

The intensity at $\boldsymbol{Q} = \boldsymbol{c}^*/2$ for the stage-1 $CoCl_2$ GIC is predicted to vary with temperature as

$$I(T) = \int_T^\infty I_0 \left(1 - \frac{T}{T_c}\right)^{2\beta} f(T_c)\, \mathrm{d}T_c \tag{24}$$

where I_0 is a constant. The least-squares fit of the intensity at $\boldsymbol{Q} = \boldsymbol{c}^*/2$ versus T to (24) yields the values $\beta = 0.125$, $\langle T_c \rangle = 9.53$ K and $\sigma = 0.71$ K. Note that the temperature derivative of the intensity at $\boldsymbol{Q} = \boldsymbol{c}^*/2$ clearly shows a broad peak at 9.53 K which coincides with $\langle T_c \rangle$.

Table 2. The critical exponent (β), T_c-distribution width (σ), average critical temperature $\langle T_c \rangle$, and $\Delta\tilde{\rho}$ for stage-1 $Co_cM_{1-c}Cl_2$ GICs, where $\Delta\tilde{\rho} = (\zeta_{sat}/\zeta_{min} - 1) \times 100$ (%), and ζ_{sat} and ζ_{min} are the values of ζ at a temperature far below T_c and at just above T_c, respectively.

Sample name	β	σ (K)	$\langle T_c \rangle$ (K)	$\Delta\tilde{\rho}$ (%)
$CoCl_2$ GIC	0.079	0.62	8.85	9.7
$Co_{0.90}Mn_{0.10}Cl_2$ GIC	0.031	0.82	7.22	0.05
$Co_{0.85}Mn_{0.15}Cl_2$ GIC	0.087	0.71	6.06	0.7
$Co_{0.95}Mg_{0.05}Cl_2$ GIC	0.084	1.11	8.59	1.5
$Co_{0.90}Mg_{0.10}Cl_2$ GIC	0.078	0.75	6.85	3.1

Ikeda *et al* [29] have shown that for the stage-1 $CoCl_2$ GIC the magnetic diffuse scattering intensity at around $\boldsymbol{Q} = \boldsymbol{c}^*/2$ is much weaker than the antiferromagnetic Bragg intensity at $\boldsymbol{Q} = \boldsymbol{c}^*/2$ partly because of the 3D long-range spin order below T_c. This implies that the contribution of the static spin correlation between adjacent $CoCl_2$ layers to the in-plane resistivity is assumed to be negligibly small. Therefore it follows that the magnetic contribution of in-plane resistivity for the stage-1 $CoCl_2$ GIC can be described by $\rho_s \simeq A'|t|^{2\beta}$ for $T < T_c$. When the smearing of T_c defined by (23) is also taken into account, the magnetic contribution of the normalized in-plane resistivity $\zeta_s(T)$ can be

expressed by

$$\zeta_s(T) = \int_T^\infty \zeta_0' \left(1 - \frac{T}{T_c}\right)^{2\beta} f(T_c)\, \mathrm{d}T_c \tag{25}$$

where ζ_0' is a constant. In terms of (25) we analyse our experimental ζ–T data for stage-1 $Co_cMn_{1-c}Cl_2$ GICs with $c = 1$, 0.90, and 0.85, and stage-1 $Co_cMg_{1-c}Cl_2$ GICs with $c = 0.95$ and 0.90. The least-squares fit of these data to (25) yields the values of β, $\langle T_c \rangle$ and σ listed in table 2. The critical exponent β thus obtained ($0.002 \leqslant \beta \leqslant 0.087$) is smaller than that estimated from the neutron scattering intensity at $\boldsymbol{Q} = \boldsymbol{c}^*/2$, but is in good agreement with that derived from the magnetization of stage-2 $Co_cMn_{1-c}Cl_2$ GICs in the presence of a magnetic field of 100 Oe: $\beta = 0.082$ for $c = 1$, 0.085 for $c = 0.90$, 0.040 for $c = 0.85$, 0.085 for $c = 0.80$, 0.046 for $c = 0.70$, and 0.107 for $c = 0.55$ [13]. These results indicate that the magnetic contribution of in-plane resistivity for stage-1 $Co_cM_{1-c}Cl_2$ GICs is proportional to the square of the staggered magnetization defined by $\langle \boldsymbol{S}_{\boldsymbol{Q}=\boldsymbol{c}^*/2} \rangle$.

The situation is very different for the stage-2 $CoCl_2$ GIC with the c-axis repeat distance $d = 12.79$ Å [13]. The interplanar distance between the graphite layer and the N.N.N. $CoCl_2$ layer (=8.07 Å) via the intervening graphite layer is much larger than that between the graphite layer and the N.N. $CoCl_2$ layer (=4.72 Å). The π-electrons in the graphite layer are scattered by spin fluctuations with the $\boldsymbol{Q} = 0$ mode for Co^{2+} spins in the N.N. $CoCl_2$ layer through the π–d exchange interaction. Our model described in section 3 predicts that the spin fluctuations with the $\boldsymbol{Q} = 0$ mode do not make any significant contribution to the resistivity because of the factor $1 - \cos\theta$ being zero in (11). This prediction seems to be inconsistent with a resistivity anomaly of the stage-2 $CoCl_2$ GIC near T_c which has been reported by Yeh *et al* [2]: the magnetic contribution for the resistivity shows a small peak at T_c. Note that similar behaviour is also observed for ζ versus T for the $Ni_cMn_{1-c}Cl_2$ GIC with $c = 0.85$ consisting of majority stage-2 with minority stage-1 and stage-3 GICs [31]. The resistivity ζ shows a kink-like behaviour at around 10 K, which is between T_c = 9.58 K for $c = 0.80$ and 14.34 K for $c = 0.90$ derived from the ac magnetic susceptibility of stage-2 $Ni_cMn_{1-c}Cl_2$ GICs [32].

Here we consider how such a resistivity anomaly in a stage-2 $CoCl_2$ GIC can be explained within the framework of our model. In our model the Co^{2+} spins are 2D ferromagnetically aligned over the whole intercalate layer below T_c. The intercalate layers are formed of small islands whose peripheries provide acceptor sites for electrons transferred from graphite layers. The 2D spin correlation length ξ increases on approaching T_c from the high-temperature side. The growth of ξ is limited by the existence of these small islands, forming a ferromagnetic cluster. It has been revealed through a SQUID magnetization measurement [12] that the low-temperature ordered phase below T_c corresponds to a cluster glass phase where the spin directions of ferromagnetic clusters are frozen due to frustrated inter-island interactions consisting of inter-island dipole–dipole interactions and interplanar antiferromagnetic interactions. The π-electrons may be scattered by the spin fluctuations of these ferromagnetic clusters. Suppose that the corresponding spin correlation function $\Gamma(\boldsymbol{Q})$ is described by the same form as (17), where $\boldsymbol{Q}_0$ is a characteristic wave vector characterizing the spin structures of ferromagnetic clusters with frozen spin directions. Then the in-plane resistivity may be described by (18) for $T > T_c$ and the second term of (20) for $T < T_c$. Since $\eta = \eta' \simeq 0$, the resistivity diverges as $|t|^{-\nu}$ for $T > T_c$ and as $|t|^{-\nu'}$ for $T < T_c$ on approaching T_c, where $\nu = \nu' = 1$ is expected for 2D XY spin systems. This divergence of the resistivity at T_c may be greatly reduced by the scattering effect related to the limited electron mean free path as described in section 3.

5.2. The critical temperature of stage-1 $Co_cMg_{1-c}Cl_2$ GICs

The percolation behaviour of $Co_cMg_{1-c}Cl_2$ GICs has been studied by Nicholls and Dresselhaus [9] for stage-1 and by Suzuki *et al* [11] for stage-2 GICs. The critical temperature T_c decreases with the substitution for Co^{2+} ions with nonmagnetic Mg^{2+} ions and reduces to zero below the percolation threshold c_p: $c_p = 0.65$ for stage-1 [9] and $c_p \simeq 0.5$ for stage-2 GICs [11]. The threshold concentration c_p is theoretically predicted as $c_p = 0.5$ for the 2D triangular lattice. Below c_p there is no long-range spin order at any temperatures above 0 K.

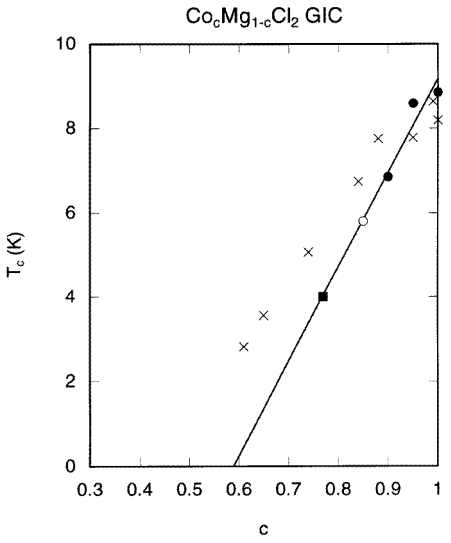

Figure 8. The critical temperature T_c versus the Co concentration for $Co_cMg_{1-c}Cl_2$ GICs: stage-1 (● and ○) from resistivity measurements and stage-2 (□) from ac magnetic susceptibility [11]. The data marked ■ are taken from [9].

Here we discuss the percolation behaviour of stage-1 $Co_cMg_{1-c}Cl_2$ GICs based on our resistivity results. Figure 8 shows the critical temperature T_c versus Co concentration for stage-1 $Co_cMg_{1-c}Cl_2$ GICs, where T_c for $c = 1$, 0.95, and 0.90 (closed circles) corresponds to the peak temperature of $-d\zeta/dT$, T_c for $c = 0.85$ (open circle) corresponds to the kink temperature of ζ, and T_c for $c = 0.77$ (closed square) is the temperature at which ζ has a minimum: $T_c \simeq 4$ K [9]. The least-squares fit of the data yields the solid straight line in figure 8. The percolation threshold c_p is estimated to be $c_p = 0.59$ from the extrapolation of the solid straight line to the $T_c = 0$ axis. This value of c_p is a little larger than the value of c_p (=0.5) predicted for the 2D triangular lattice, but is smaller than the value of c_p (=0.65) obtained by Nicholls and Dresselhaus [9]. The deviation of c_p from the theoretical value is partly attributed to the random distribution of in-plane voids caused by the incomplete in-plane filling factor of the GICs [9]: Co^{2+} ions are replaced by both nonmagnetic Mg^{2+} ions and voids. In figure 8, for comparison, we show the T_c–c data for stage-2 $Co_cMg_{1-c}Cl_2$ GICs determined from the ac magnetic susceptibility [11]. The value of T_c for the stage-1 compounds is lower than that for the stage-2 compounds with the same concentration for $c < 0.90$. The dimensionality of these systems decreases from 2D-like for stage-2 to 3D-like for stage-1 GICs due to the decrease in the interplanar distance, predicting an increase of T_c with decreasing stage number. The difference between our results and this prediction

can be explained if the number of voids per intercalate layer for a stage-1 GIC is much larger than that for a stage-2 GIC.

5.3. The concentration dependence of $\Delta\tilde{\rho}$ in stage-1 $Co_cM_{1-c}Cl_2$ GICs

We discuss the Co concentration dependence of $\Delta\tilde{\rho}$. For stage-1 $Co_cMn_{1-c}Cl_2$ GICs $\Delta\tilde{\rho}$ decreases from 9.7% for $c = 1$ to $\simeq$0% for $c = 0.7$ with decreasing Co concentration. For stage-1 $Co_cMg_{1-c}Cl_2$ GICs, $\Delta\tilde{\rho}$ also decreases from 9.7% for $c = 1$ to $\simeq$0% for $c = 0.85$ with decreasing Co concentration.

Our model described in section 3 predicts that the occurrence of $\Delta\tilde{\rho}$ below T_c is due to the scattering of π-electrons by antiferromagnetic in-plane spin configurations consisting of the superposition of the in-plane ferromagnetic spin structures of the N.N. intercalate layers separated by the graphite layer. The important conditions for the occurrence of $\Delta\tilde{\rho}$ below T_c in stage-1 $Co_cM_{1-c}Cl_2$ GICs are that (i) the effective antiferromagnetic interplanar exchange interaction J'_{eff} should be rather strong and that (ii) the antiferromagnetic spin alignment of the superimposed in-plane ferromagnetic spin structure should be described by a well-defined antiferromagnetic Bragg point at $\boldsymbol{Q} = \boldsymbol{Q}_0$. The latter condition also implies that the intercalate layers are structurally correlated along the c-axis.

First we consider the magnitude of $\Delta\tilde{\rho}$ for the stage-1 $Co_cM_{1-c}Cl_2$ GICs. In these systems the 3D long-range spin order appears at k_BT_c where the thermal energy (k_BT) is of the same order as $|J'_{eff}|$. In other words, the value of T_c is a measure for J'_{eff} which is described by

$$J'_{eff} = p(c)J'S(S+1)\left(\frac{\xi}{a}\right)^2. \tag{26}$$

Here J' is the antiferromagnetic interplanar exchange interaction and a is the in-plane lattice constant of the intercalate layer. The parameter $p(c)$ is the probability of the overlap of the ordered region, with the area of $\simeq \pi\xi^2$, in one intercalate layer, with another region, with the same area, in the adjacent intercalate layer. For stage-1 $Co_cMn_{1-c}Cl_2$ GICs and $Co_cMg_{1-c}Cl_2$ GICs, T_c drastically decreases with decreasing Co concentration (table 2 and figure 8), leading to the reduction of $\Delta\tilde{\rho}$. The ratio $|J'_{eff}(c)|/|J'_{eff}(c=1)|$ decreases to 1/2 at $c = 0.70$ for stage-1 $Co_cMn_{1-c}Cl_2$ GICs and at $c = 0.77$ for stage-1 $Co_cMg_{1-c}Cl_2$ GICs. Since J' is considered to be independent of the Co concentration, it follows that ξ and $p(c)$ in (26) decrease with decreasing Co concentration. The decrease of ξ in stage-1 $Co_cMn_{1-c}Cl_2$ GICs is due to the spin frustration effect arising from a competition between the intraplanar ferromagnetic exchange interaction J(Co–Co) and the antiferromagnetic exchange interaction J(Mn–Mn). The decrease of ξ in stage-1 $Co_cMg_{1-c}Cl_2$ GICs corresponds to the breakdown of ordered regions of Co^{2+} spins by the replacement of Co^{2+} ions by nonmagnetic Mg^{2+} ions. Thus the reduction of $\Delta\tilde{\rho}$ for $c < 0.9$ in stage-1 $Co_cMn_{1-c}Cl_2$ GICs and $Co_cMg_{1-c}Cl_2$ GICs is attributed to the decrease of ξ and $p(c)$ with decreasing Co concentration. The superimposed in-plane spin structure of these compounds with $c > 0.9$ is considered to be still similar to that of the stage-1 $CoCl_2$ GIC. Note that the intercalate layers of stage-1 $Co_cMn_{1-c}Cl_2$ GICs are expected to stack in an ordered abgabg rhombohedral sequence, since the c-axis stacking sequences of the stage-1 $CoCl_2$ GIC and the stage-1 $MnCl_2$ GIC are described by the same sequence [14].

6. Conclusion

We have studied the temperature dependence of the in-plane resistivity for stage-1 $Co_cMn_{1-c}Cl_2$ GICs and stage-1 $Co_cMg_{1-c}Cl_2$ GICs near T_c. We have found that the resistivity shows a drastic increase below T_c with decreasing temperature. The temperature dependence of this resistivity anomaly is similar to that of the square of the staggered magnetization with a smeared power law with exponent 2β. We have presented a model which can explain this resistivity anomaly: the π-electrons are scattered by the spin fluctuation of the antiferromagnetic in-plane spin configuration arising from the superposition of two ferromagnetic in-plane spin structures. The π-electrons experience two types of molecular field whose directions are antiparallel to each other. The key point of our model is that (i) for π-electrons there is no distinction between the π–d exchange interaction effect from one of the N.N. intercalate layers and that from the other N.N. intercalate layer, and that (ii) the intercalate layers are structurally correlated with each other along the c-axis.

We have also discussed the Co concentration dependence of T_c for stage-1 and stage-2 $Co_cMg_{1-c}Cl_2$ GICs. The percolation threshold is estimated to be $c_p = 0.59$, which is a little larger than the theoretical value for the 2D triangular lattice (=0.50). The critical temperature T_c for stage-1 compounds is lower than that for stage-2 compounds with the same Co concentration. These results give indirect evidence that the number of voids per intercalate layer for stage-1 compounds is much larger than that for stage-2 compounds with the same Co concentration.

Acknowledgments

We would like to thank K Sugihara for directing our interest to studies on the electrical resistivity of stage-1 RMGICs, and H Suematsu and Y Hishiyama for providing us with high-quality single-crystal kish graphites. We are grateful to L F Tien, C J Hsieh, N Inadama, J Morillo, and F Khemai for their help with sample preparation and characterization, and A Tafti and A Turrell for their help with the resistivity measurements. This work was supported by the National Science Foundation, grant No DMR-9201656.

References

[1] Issi J P 1992 *Graphite Intercalation Compounds II* ed H Zabel and S A Solin (Berlin: Springer) pp 195–245
[2] Yeh N C, Sugihara K, Dresselhaus M S and Dresselhaus G 1989 *Phys. Rev.* B **40** 622–35
[3] Kinany-Alaoui M, Piraux L, Bayot V, Issi J P, Pernot P and Vangelisti R 1989 *Synth. Met.* **34** 537–42
[4] Pernot P and Vangelisti R 1989 *Z. Naturf.* b **44** 761–6
[5] McRae E, Herold A, LeLaurain M, Mareche J F, Perignon A, Pernot P and Vangelisti R 1988 *Symp. on Graphite Intercalation Compounds at the Materials Research Society Meeting (Boston, MA, 1988)* ed M Endo, M S Dresselhaus and G Dresselhaus (Pittsburgh, PA: Materials Research Society Press) extended abstracts, pp 105–8
[6] Piraux L 1994 *Mol. Cryst. Liq. Cryst.* **245** 67–74
[7] Nicholls J T, Speck J S and Dresselhaus G 1989 *Phys. Rev.* B **39** 10 047–55
[8] Nicholls J T and Dresselhaus G 1990 *J. Phys.: Condens. Matter* **2** 8391–404
[9] Nicholls J T and Dresselhaus G 1990 *Phys. Rev.* B **41** 9744–51
[10] Sugihara K, Yeh N C, Dresselhaus M S and Dresselhaus G 1989 *Phys. Rev.* B **39** 4577–87
[11] Suzuki I S, Hsieh C J, Khemai F, Burr C R and Suzuki M 1993 *Phys. Rev.* B **47** 845–55
[12] Suzuki I S, Suzuki M and Maruyama Y 1993 *Phys. Rev.* B **48** 13 550–8
[13] Suzuki I S, Suzuki M, Tien L F and Burr C R 1991 *Phys. Rev.* B **43** 6393–404
[14] Speck J S, Nicholls J T, Wuensch B J, Delgado J M, Dresselhaus M S and Miyazaki H 1991 *Phil. Mag.* B **64** 181–206
[15] Wiesler D G, Suzuki M and Zabel H 1987 *Phys. Rev.* B **36** 7051–62

[16] Dresselhaus G, Nicholls J T and Dresselhaus M S 1992 *Graphite Intercalation Compounds II* ed H Zabel and S A Solin (Berlin: Springer) pp 247–345
[17] Suzuki M 1990 *Crit. Rev. Solid State Mater. Sci.* **16** 237–54
[18] Kamimura H, Nakao K, Ohno T and Inoshita T 1980 *Physica* B+C **99** 401–5
[19] de Gennes P G and Friedel J 1958 *J. Phys. Chem. Solids* **4** 71–7
[20] Kim D J 1964 *Prog. Theor. Phys.* **31** 921–3
[21] Fisher M E and Langer J S 1968 *Phys. Rev. Lett.* **20** 665–8
[22] Coqblin B 1977 *The Electronic Structure of Rare-Earth Metals and Alloys: the Magnetic Heavy Rare-Earths* (New York: Academic) pp 22–34
[23] Richards P M and Salamon M B 1974 *Phys. Rev.* B **9** 32–45
[24] Marshall W and Lowde S W 1971 *Theory of Thermal Neutron Scattering* (Oxford: Clarendon) pp 173–252
[25] Collins M F 1989 *Magnetic Critical Scattering* (New York: Oxford University Press) pp 12–30
[26] Suzuki M, Ikeda H and Endoh Y 1983 *Synth. Met.* **8** 43–51
[27] Sugihara K 1995 private communication
[28] Barati M, Ummat P K and Datars W R 1993 *Phys. Rev.* B **48** 15 316–9
[29] Ikeda H, Endoh Y and Mitsuda S 1985 *J. Phys. Soc. Japan* **54** 3232–5
[30] Birgeneau R J, Als-Nielsen J and Shirane G 1977 *Phys. Rev.* B **16** 280–92
[31] Suzuki M, Suzuki I S, Olson B and Shima T 1995 unpublished
[32] Suzuki I S, Khemai F, Suzuki M and Burr C R 1992 *Phys. Rev.* B **45** 4721–8